Nanoscale

PAPER

View Article Online
View Journal | View Issue

Cite this: *Nanoscale*, 2017, **9**, 15107

Pt–Ag cubic nanocages with wall thickness less than 2 nm and their enhanced catalytic activity toward oxygen reduction†

Xiaojun Sun,[a] Xuan Yang,[b] Yun Zhang,[a] Yong Ding,[a] Dong Su[c] and Dong Qin*[a]

Received 17th June 2017,
Accepted 8th September 2017

DOI: 10.1039/c7nr04366j

rsc.li/nanoscale

We report a facile synthesis of Pt–Ag nanocages with walls thinner than 2 nm by depositing a few atomic layers of Pt as conformal shells on Ag nanocubes and then selectively removing the Ag template *via* wet etching. In a typical process, we inject a specific volume of aqueous H_2PtCl_6 into a mixture of Ag nanocubes, ascorbic acid (H_2Asc), NaOH, and poly(vinylpyrrolidone) in water under ambient conditions. At an initial pH of 11.9, the Pt(IV) precursor is quickly reduced by an ascorbate monoanion, a strong reducing agent derived from the neutralization of H_2Asc with NaOH. The newly formed Pt atoms are deposited onto the edges and then corners and side faces of Ag nanocubes, leading to the generation of Ag@Pt core–shell nanocubes with a conformal Pt shell of approximately three atomic layers (or, about 0.6 nm in thickness) when 0.4 mL of 0.2 mM H_2PtCl_6 is involved. After the selective removal of Ag in the core using an etchant based on a mixture of $Fe(NO_3)_3$ and HNO_3, we transform the core–shell nanocubes into Pt–Ag alloy nanocages with an ultrathin wall thickness of less than 2 nm. We further demonstrate that the as-obtained nanocages with a composition of $Pt_{42}Ag_{58}$ exhibit an enhanced catalytic activity toward the oxygen reduction reaction, with a mass activity of 0.30 A mg^{-1} and a specific activity of 0.93 mA cm^{-2}, which are 1.6 and 2.5 times, respectively, greater than those of a commercial Pt/C catalyst.

Introduction

Platinum is a catalyst widely used for many important reactions, including CO oxidation in catalytic converters,[1] electrooxidation of small organic fuels such as formic acid and ethanol,[2] and oxygen reduction reaction (ORR), key to the operation of proton-exchange membrane fuel cells.[3,4] However, the expensive price and low abundance associated with Pt present a major challenge for developing cost-effective products. One approach to reduce the loading of Pt is to switch from the conventional solid nanoparticles to more open nanostructures with hollow interiors and porous walls such as Pt-based nanocages.[5] In this structure, most of the Pt atoms, including those located on the inner surface, can participate in the catalytic reaction, making it possible to achieve high specific surface areas without using extremely small particles that are highly susceptible to sintering and/or dissolution from the support.

Three different strategies have been reported in the literature for the fabrication of Pt-based nanocages. The first approach relies on the overgrowth of Pt conformal shells on well-defined Pd nanocrystal seeds for the generation of Pd@Pt_{nL} (n = 1–6) core–shell nanocrystals, followed by the removal of Pd cores. To this end, Xia and other groups have demonstrated the fabrication of Pt-based nanocages by templating with Pd nanocubes,[5] octahedra,[6] decahedra,[7] and icosahedra.[8,9] The second approach exploits the galvanic replacement reaction between a Pt(II) precursor and a sacrificial template made of Ag.[10–13] In this case, Pt atoms are produced from a Pt(II) precursor at the expense of Ag atoms for their deposition onto the surface of a Ag template, leading to the formation of a nanobox and then a nanocage through the interplay of alloying and dealloying between Pt and Ag. The third approach starts with the co-reduction of Pt(II) and Pd(II) precursors to generate Pt-on-Pd bimetallic nanodendrites comprised of a Pd interior and a dendritic Pt exterior.[14,15] After chemical etching of the Pd interior, Pt–Pd bimetallic hollow nanoparticles with dendritic shells are obtained.[16,17] Among these three strategies, the first one is particularly attractive as it allows for the deposition of an ultrathin, conformal shell of Pt on Pd nanocrystals with a thickness precisely controllable

[a]*School of Materials Science and Engineering, Georgia Institute of Technology, Atlanta, Georgia 30332, USA. E-mail: dong.qin@mse.gatech.edu*
[b]*The Wallace H. Coulter Department of Biomedical Engineering, Georgia Institute of Technology and Emory University, Atlanta, Georgia 30332, USA*
[c]*Center for Functional Nanomaterials Brookhaven National Laboratory Upton, New York, 11973, USA*

†Electronic supplementary information (ESI) available. See DOI: 10.1039/c7nr04366j

down to the atomic scale. It has also been demonstrated that the Pt-based nanocages with subnanometer-thick walls exhibited great catalytic performance toward ORR.[5–9] Despite the remarkable success, however, the Pt coating process involves a polyol solvent at an elevated temperature above 200 °C. It is also rather expensive to use another scarce precious metal such as Pd as the sacrificial template.

One solution to further reduce the cost associated with Pt-based nanocages is to replace Pd with Ag as the sacrificial template. Unfortunately, it has been difficult to simply extend the standard protocol developed for the conformal deposition of Pt on Pd seeds to Ag nanocrystals due to the involvement of galvanic replacement between Ag and a Pt(II) or Pt(IV) precursor.[10–13] In this case, the Ag nanocrystal seed can be destructed to such an extent that it can no longer serve as a physical template to direct the conformal deposition of Pt. Over the past few years, we have established the scientific basis and rules for achieving galvanic replacement-free overgrowth of Au or Pd on Ag seeds.[18–21] Our strategy is based on the introduction of a faster parallel reaction to compete with and thereby suppress the galvanic replacement reaction. Herein, we demonstrate that the same principle can be extended to deposit conformal, ultrathin shells of Pt on the surface of Ag nanocubes for the generation of Ag@Pt core–shell nanocubes with a shell thickness as thin as three atomic layers. The facile synthesis involves the injection of H_2PtCl_6 (a precursor to elemental Pt) into an aqueous suspension of Ag nanocubes in the presence of ascorbic acid (H_2Asc), poly(vinylpyrrolidone) (PVP, a colloidal stabilizer), and NaOH at an initial pH of 11.9 under ambient conditions. Upon the removal of Ag cores with etching by using a mixture of $Fe(NO_3)_3$ and HNO_3, the core–shell nanocubes can be transformed into Pt-based cubic nanocages with a wall thickness thinner than 2 nm. Upon deposition on carbon, the nanocages with a composition of $Pt_{42}Ag_{58}$ are found to exhibit enhanced catalytic activity toward ORR, with mass and specific activities of 0.30 A mg^{-1} and 0.93 mA cm^{-2}, respectively.

Experimental

Chemicals and materials

Silver trifluoroacetate (CF_3COOAg, 98%), chloroplatinic acid hexahydrate ($H_2PtCl_6{\cdot}6H_2O$, 99.9+%), aqueous hydrochloric acid (HCl, 37%), sodium hydrosulfide hydrate ($NaHS{\cdot}xH_2O$), sodium borohydride ($NaBH_4$), H_2Asc (99%), sodium hydroxide (NaOH, 98+%), potassium tetrachloroplatinate(II) (K_2PtCl_4, 99.9+%), iron(III) nitrate nonahydrate ($Fe(NO_3)_3{\cdot}9H_2O$), nitric acid (HNO_3, 70%), and PVP with an average molecular weight of 29 000 (PVP-29) or 55 000 (PVP-55) were all acquired from Sigma-Aldrich. Ethylene glycol (EG) was purchased from J. T. Baker. All chemicals were used as received. Deionized (DI) water with a resistivity of 18.2 MΩ cm at room temperature was used throughout all experiments. The commercial Pt/C catalyst was obtained from Tanaka Kikinzoku Kogyo.

Synthesis of Ag nanocubes

We synthesized the Ag nanocubes with an edge length of 38.6 ± 1.3 nm by following the protocol developed by Xia and co-workers.[22] The nanocubes were washed with acetone and water three times, and then dispersed in water for storage and further use.

Synthesis of Ag@Pt core–frame and core–shell nanocubes

In a standard protocol, 2 mL of aqueous PVP-29 (1 mM), 0.5 mL of aqueous H_2Asc (0.1 M), and 0.5 mL of NaOH (0.2 M) were mixed in a 23 mL glass vial under magnetic stirring, followed by the introduction of 13.4 μL of the aqueous suspension of Ag nanocubes (with a final concentration of 4.2×10^{10} particles per mL). Afterwards, a specific amount (0.01, 0.1, or 0.4 mL) of aqueous H_2PtCl_6 (0.2 mM) or K_2PtCl_4 (0.2 mM) was injected into the mixture in one shot. The mixture was kept at room temperature for another 2 h before the products were collected by centrifugation at 5500 rpm for 15 min, washed twice with water, and then dispersed in water for further use.

Selective etching of Ag cores from the Ag@Pt core–frame and core–shell nanocubes

We prepare an aqueous solution by mixing $Fe(NO_3)_3$ (1 mM) with HNO_3 (3 mM) at a 1 : 1 volume ratio. The as-prepared Ag@Pt nanocubes were collected and dispersed in 0.1 mL of water, followed by the addition of 1 mL of the $Fe(NO_3)_3/HNO_3$ mixture and incubated at room temperature for 1 h. The final products were collected by centrifugation at 14 000 rpm for 20 min, followed by washing twice with water and re-dispersed in water for further characterization.

XPS analysis of the Ag@Pt core–frame and core–shell nanocubes

Approximately 25 μL of the as-obtained sample was drop cast on the surface of a silicon substrate and allowed to dry overnight in air. The sample was then analyzed using X-ray photoelectron spectroscopy. The Pt 4f (65–85 eV) and Ag 3d (360–380 eV) peaks of the sample were measured with a resolution of 0.1 eV.

Instrumentation and characterization

We collected all the samples using a conventional centrifuge (Eppendorf 5430). The pH value was measured by using a FiveEasy pH Meter (Mettler Toledo, Columbus, OH). The contents of Pt and Ag were determined using an inductively coupled plasma mass spectrometer (ICP-MS, NexION 300Q, PerkinElmer, Waltham, MA). XPS was performed on a Thermo K-Alpha X-ray photoelectron spectrometer (Thermo Fisher Scientific, Waltham, MA). Transmission electron microscopy (TEM) images were taken using an HT7700 microscope (Hitachi, Tokyo, Japan) operated at 120 kV. High angle annular dark field scanning transmission electron microscopy (HAADF-STEM) imaging and electron energy loss spectroscopy (EELS) mapping were conducted on a Hitachi HD2700 STEM operated at 200 kV and equipped with a probe aberration corrector.

Electrochemical measurements

Firstly, 0.5 mg of carbon-supported Pt–Ag nanocages were dispersed in a mixture of 0.8 mL of water, 0.2 mL of isopropanol, and 10 μL of 5% Nafion under ultrasonication for 1 h to produce an ink for electrochemical measurements. Next, 10 μL of the suspension was cast on a glassy carbon rotating disk electrode (RDE, Pine Research Instrumentation) with a geometric area of 0.196 cm^2, followed by drying under ambient conditions at room temperature. With the same preparation procedure, the commercial Pt/C catalyst (46.6 wt%, *ca.* 2.1 nm Pt particles supported on Ketjenblack EC-300J, Tanaka Kikinzoku Kogyo) was used as a benchmark for comparison. Electrochemical measurements were conducted using a CHI 600E potentiostat (CH Instruments). A Hydroflex hydrogen reference electrode (Gaskatel) and a Pt mesh were used as the reference and counter electrodes, respectively. All potentials were converted to values with reference to the reversible hydrogen electrode (RHE). The electrolyte (0.1 M $HClO_4$) was prepared by diluting a 70% stock solution with water. The cyclic voltammetric (CV) curves were recorded at room temperature in a N_2-saturated 0.1 M $HClO_4$ solution in the potential range of 0.08–1.1V_{RHE} at a scanning rate of 50 mV s^{-1}. We calculated the electrochemical active surface areas (ECSA) of each catalyst based on the charges associated with the desorption of hydrogen in the region of 0.08–0.45V_{RHE} after double-layer correction with a reference value of 210 μC cm^{-2} (for commercial Pt/C and Pt–Ag nanocages) for the desorption of a monolayer of hydrogen from the Pt surface. We measured the ORR activities at room temperature in the potential range of 0.08–1.1V_{RHE} in an O_2-saturated 0.1 M $HClO_4$ solution using the RDE method at a scanning rate of 10 mV s^{-1} (rotating speed at 1600 rpm). The background current is measured in the potential range of 0.08–1.1V_{RHE} by running the ORR sweep profile in a N_2-saturated 0.1 M $HClO_4$ solution at a scanning rate of 10 mV s^{-1} (rotating speed at 1600 rpm). The ORR data were corrected by ohmic iR drop compensation and background currents. The kinetic current density (j_K) was derived from the Koutecky–Levich equation:

$$\frac{1}{j} = \frac{1}{j_K} + \frac{1}{j_L},$$

where j is the measured current density and j_L is the diffusion-limiting current density. For the accelerated durability test, we collected CVs and ORR polarization curves after sweeping 5000 cycles in the potential range of 0.6–1.1V_{RHE} in an O_2-saturated 0.1 M $HClO_4$ solution using the RDE method at a scanning rate of 0.1 mV s^{-1}. After the test, the particles were removed from the electrode by sonication and then dissolved in 0.5 mL aqua regia for ICP-MS analysis.

Results and discussion

Fig. 1 outlines a pathway proposed to account for the deposition of Pt on a Ag nanocube under ambient conditions. Because NaOH is used to adjust the initial pH of the reaction solution to the alkaline region, the hydroxide can affect the deposition of Pt atoms on Ag nanocubes in a number of different ways. First of all, the added H_2PtCl_6 is supposed to be quickly neutralized to generate $PtCl_6^{2-}$, followed by possible ligand exchange with H_2O and OH^- to generate Pt(IV) species that may include $PtCl_5(OH)^{2-}$ and $PtCl_4(OH)_2^{2-}$.[23–26] However, as confirmed by the UV-vis spectra shown in Fig. S1,† the Pt(IV) ions quickly formed stable complexes with the nitrogen atoms in PVP,[26] preventing them from further ligand exchange with H_2O and OH^-. On the other hand, H_2Asc was neutralized to generate an ascorbate monoanion ($HAsc^-$), a strong reducing agent, for the quick production of Pt atoms through direct

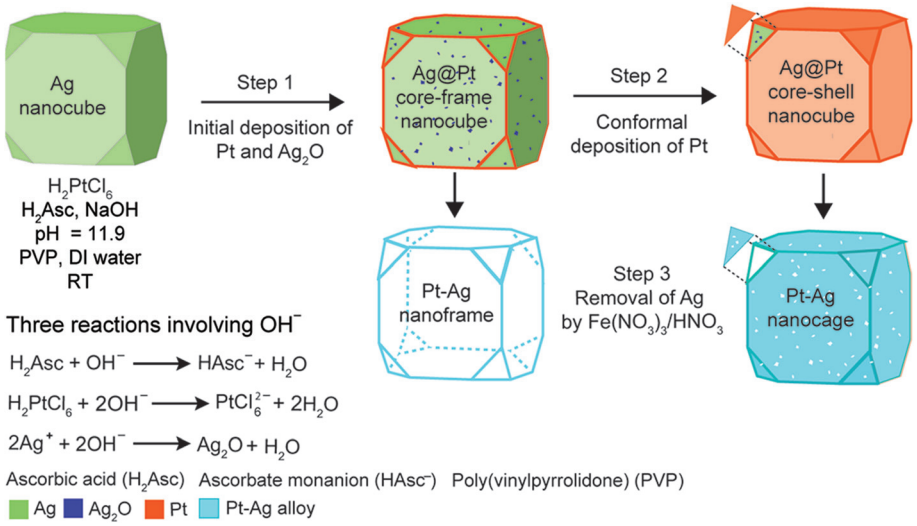

Fig. 1 Schematic illustration of a mechanism proposed to account for the deposition of Pt on the surface of a Ag nanocube as the volume of the injected Pt(IV) precursor is increased, corresponding to the Pt–Ag nanoframe and nanocage after the removal of Ag in the core.

chemical reduction.[27] As a result, the galvanic replacement reaction would become less favorable, making the reduction of Pt(IV) by $HAsc^-$ a dominant channel for the generation of Pt atoms. Finally, any Ag^+ ions released from the Ag nanocubes due to oxidative etching can react with OH^- in the reaction solution instantaneously, resulting in the formation of Ag_2O patches on the surface of the Ag nanocubes.[27]

Because the surface free energies of the low-index facets on Ag nanocubes decrease in the order of $\gamma_{(110)} > \gamma_{(111)} > \gamma_{(100)}$ in the presence of PVP, it is anticipated that the Pt atoms derived from the chemical reduction of Pt(IV) by $HAsc^-$ should be sequentially deposited on the edges, corners, and side faces for the formation of Ag@Pt core–frame and then core–shell nanocubes. Immediately after the injection of H_2PtCl_6 into the reaction solution, we suspect that $PtCl_6^{2-}$ derived from the neutralization by NaOH could also react with Ag nanocubes for the initial deposition of Pt atoms on the edges of Ag nanocubes at the expense of Ag atoms located at the corners or side faces of the nanocubes. As a consequence, the Ag^+ ions released from the nanocubes can instantaneously react with the surrounding OH^- ions to generate Ag_2O patches sporadically on the corners or side faces, preventing the underlying Ag atoms from further oxidation through the galvanic replacement reaction. Afterwards, the Pt atoms should be mainly produced through the chemical reduction by $HAsc^-$, followed by their deposition onto the edges for the generation of Ag@Pt core–frame nanocubes with Ag_2O patches at the corner sites of the nanocubes. If the synthesis is continued with a larger injection volume of aqueous H_2PtCl_6, the side faces and corners of the nanocubes can also be covered by Pt atoms through direct deposition and/or surface diffusion from the edges. Because the nucleation energy barrier on the oxide patches tends to be higher than a metal surface,[27] we argue the Pt atoms should not be directly deposited on the Ag_2O regions. Instead, they should cover the surface of oxide patches *via* surface diffusion, generating an ultrathin shell of Pt on the surface of Ag nanocubes for the generation of Ag@Pt core–shell nanocubes. When the Ag_2O patches are removed with HNO_3 to lift off the Pt deposited on these regions, followed by selective etching of the Ag cores by $Fe(NO_3)_3$, the Ag@Pt core–frame and core–shell nanocubes should evolve into Pt–Ag alloy nanoframes and nanocages, respectively.

In a typical synthesis, we started with the preparation of Ag nanocubes with an average edge length of 38.6 ± 1.3 nm by following a published protocol (Fig. S2†).[22] We then dispersed the Ag nanocubes in an aqueous solution containing H_2Asc (0.1 mM), PVP (1 mM), and NaOH (0.2 M) at an initial pH set to 11.9, followed by the one-shot injection of different volumes of aqueous H_2PtCl_6 (0.2 mM) under magnetic stirring, and finally allowing them to react for 2 h at room temperature. Fig. 2A, C and E show the products obtained with the addition of 0.02, 0.1, and 0.4 mL of aqueous H_2PtCl_6, respectively. We found that the cubic morphology of the Ag nanocubes was preserved while their averaged edge length was slightly increased from 38.6 ± 1.3 nm to 38.7 ± 2.0 nm, 39.0 ± 1.7 nm, and 39.9 ± 1.8 nm, respectively. Our inductively coupled plasma mass spectrometry (ICP-MS) analyses indicate that the Pt contents were 2.3 ± 0.1% and 4.7 ± 0.2% for the two samples corresponding to the injection volumes of 0.1 and 0.4 mL, respectively. We also used X-ray photoelectron spectroscopy (XPS) to analyze the Pt deposited on the Ag nanocubes. As shown in Fig. S3,† the amount of Pt being deposited on the Ag nanocubes was increased as the injection volume of H_2PtCl_6 solution was increased from 0.02 to 0.1 mL. To confirm the essential role of NaOH in supporting the deposition of Pt on the Ag nanocubes by suppressing the galvanic replacement reaction between the Ag nanocubes and Pt(IV) precursor, we performed a control experiment by excluding NaOH while keeping all other parameters the same. As shown in Fig. S4,† we observed the formation of voids in the nanocubes, confirming the involvement of a galvanic replacement reaction. Taken together, these data confirm the conformal deposition of Pt on the Ag nanocubes. By simply changing the injection volume of

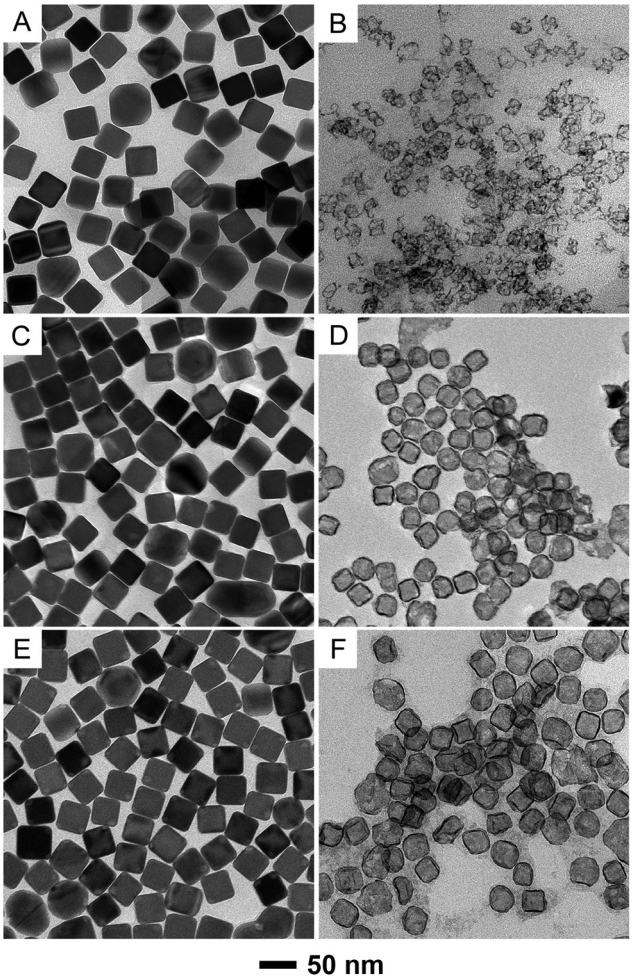

Fig. 2 TEM images of the products before (left panel) and after (right panel) etching with an aqueous solution containing $Fe(NO_3)_3$ and HNO_3. The samples were prepared by reacting Ag nanocubes with different volumes of aqueous 0.2 mM H_2PtCl_6 in the presence of H_2Asc, PVP, and NaOH at an initial pH of 11.9: (A, B) 0.02 mL, (C, D) 0.1 mL, and (E, F) 0.4 mL, respectively.

the Pt(IV) precursor, we can easily control the ratio of Pt to Ag in the products.

To reveal the deposition pathway of the Pt atoms on the surface of Ag nanocubes, we used an aqueous mixture of $Fe(NO_3)_3$ (1 mM) and HNO_3 (3 mM) to selectively etch away Ag but not Pt (see the Experimental section for details). For the injection volume of 0.02 mL, Fig. 2B shows the formation of broken nanoframes, indicating that the initial deposition of Pt indeed occurred on the edges of the Ag nanocubes, consistent with our findings in other systems.[27–29] We noticed that several of the core–frame nanocubes survived from the etching process and the size of a nanoframe was much smaller than that of the nanocubes shown in Fig. 2A. It is anticipated that the Pt atoms deposited on the edges of the Ag nanocubes only generated relatively thin ridges, and as a result, the resultant nanoframes could deform and thus shrink inward due to the capillary force involved in the drying process of TEM sample preparation. As the injection volume was increased from 0.02 to 0.1 mL, Fig. 2D shows the formation of nanocages in the presence of pores on the side surfaces. The average edge length of the nanocages was 27.2 ± 3.8 nm, *ca.* 30% smaller than that of the original nanocubes shown in Fig. 2C. Also, the cubic shape was not well preserved due to the involvement of ultrathin walls for the nanocages. With a further increase of injection volume to 0.4 mL, Fig. 2F shows the formation of well-defined nanocages with small pores on the side faces. Again, the average edge length was only 31.1 ± 3.3 nm, roughly 22% smaller than that of the original nanocubes shown in Fig. 2E. When we increased the injection volume to 0.8 mL, we obtained nanocages with an average edge length of 33.0 ± 3.9 nm, as shown in Fig. S5.† However, due to the involvement of ultrathin walls that are susceptible to deformation during sample prep and/or upon exposure to an electron beam, we were unable to resolve the exact wall thickness of the nanocages by TEM.

We also performed another control experiment to replace the Pt(IV) precursor based on H_2PtCl_6 with a Pt(II) precursor based on K_2PtCl_4, while keeping all other experimental parameters unaltered. At an injection volume of 0.4 mL, Fig. S6A and B,† show the as-obtained products before and after treatment with the $Fe(NO_3)_3/HNO_3$ etchant. The structures are similar to those shown in Fig. 2E and F. Collectively, our results support the aforementioned argument that the initial deposition of Pt atoms derived from the reduction of the Pt(II) or Pt(IV) precursor would start from the edges of the Ag nanocubes, followed by deposition on the corners and side faces, sequentially transforming the Ag nanocubes into Ag@Pt core–frame and core–shell nanocubes.

It is worth pointing out that HNO_3 in the etching solution could serve as an acid to selectively dissolve the Ag_2O patches located on the surface of the nanocubes, leading to the transformation of Ag@Pt core–frame or core–shell nanocubes into nanoframes or nanoboxes after the further removal of Ag cores by $Fe(NO_3)_3$. To support our argument that the Ag_2O patches were removed through an acid–base neutralization reaction, we performed a control experiment to etch the as-obtained Ag@Pt nanocubes prepared with an injection volume of 0.4 mL with 3% aqueous H_2O_2 etching. As shown in Fig. S7A,† there was no change in the morphology. In comparison, when the sample was treated with a weak acid such as H_2Asc and then aqueous H_2O_2, as shown in Fig. S7B,† we obtained nanocages again after the removal of Ag cores. Taken together, our results confirm the formation of Ag_2O, a base that could be readily dissolved by a protonic acid. We believe that any protonic acid can be used to dissolve the Ag_2O patches as long as it does not compromise the structural integrity of the Pt overlayers on the side faces and thus compromise the etching of Ag by $Fe(NO_3)_3$.

We also used aberration-corrected high-angle annular dark-field scanning TEM (HAADF-STEM) to characterize one of the Ag@Pt core–shell nanocubes prepared with the injection of 0.4 mL of aqueous H_2PtCl_6 (see Fig. 2E). As shown in Fig. 3A, Pt atoms could be readily resolved on the surface of the Ag nanocube due to their large difference in atomic number. It is interesting to acknowledge the presence of a shallow hole at the top right corner of the nanocube, suggesting the loss of Ag atoms due to galvanic replacement in the initial stage. Fig. 3B shows the arrangement of Ag and Pt atoms, from which we identified that 3–4 atomic layers of Pt atoms (with a thickness of about 0.6 nm) were deposited on the surface of the Ag nanocube, consistent with our aforementioned estimate based on the increase in the edge length from 38.6 ± 1.3 nm to 39.9 ± 1.8 nm. We also analyzed the elemental distributions of Ag and Pt using STEM-electron energy loss spectroscopy (EELS). Fig. 3C shows the STEM-EELS mapping of Ag, suggesting some loss of Ag at one of the corners of the nanocube. Fig. 3D shows the STEM-EELS mapping of Pt, indicating the deposition of Pt on the edges, corners, and side faces of the nanocube. Taken together, this set of data confirms the formation of $Ag@Pt_{3L}$ core–shell nanocubes when the sample was prepared with 0.4 mL of 0.2 mM aqueous H_2PtCl_6.

We further used high-resolution (HR) TEM to characterize the detailed morphology and elemental composition of one of the Pt–Ag nanocages shown in Fig. 2F. Fig. 4A shows a HAADF-STEM image of the Pt–Ag nanocages, from which we could spot the small openings across the side faces. At atomic resolution, as shown in Fig. 4B, we could only resolve the lattice fringes in some areas because the ultrathin and fragile nanocages tended to lose their original shapes after washing and centrifugation steps during the TEM sample preparation process. It is worth mentioning that the inter-diffusion and alloying process between Pt and Ag could result in the retention of some Ag atoms during the etching process, and as a result, Ag@Pt core–shell nanocubes with a shell thickness of 0.6 nm were transformed into Pt–Ag nanocages with a thickness less than 2 nm. We analyzed the elemental distributions of Ag and Pt for an individual nanocage using energy dispersive X-ray spectroscopy (EDS). Fig. 4C–F, show the STEM image of a nanocage, and the corresponding EDS mapping results of Ag and Pt, respectively. Based on the ICP-MS measurements, the nanocages can be assigned with a composition of $Pt_{42}Ag_{58}$, corresponding to a Pt and Ag atomic ratio of roughly 1.0.

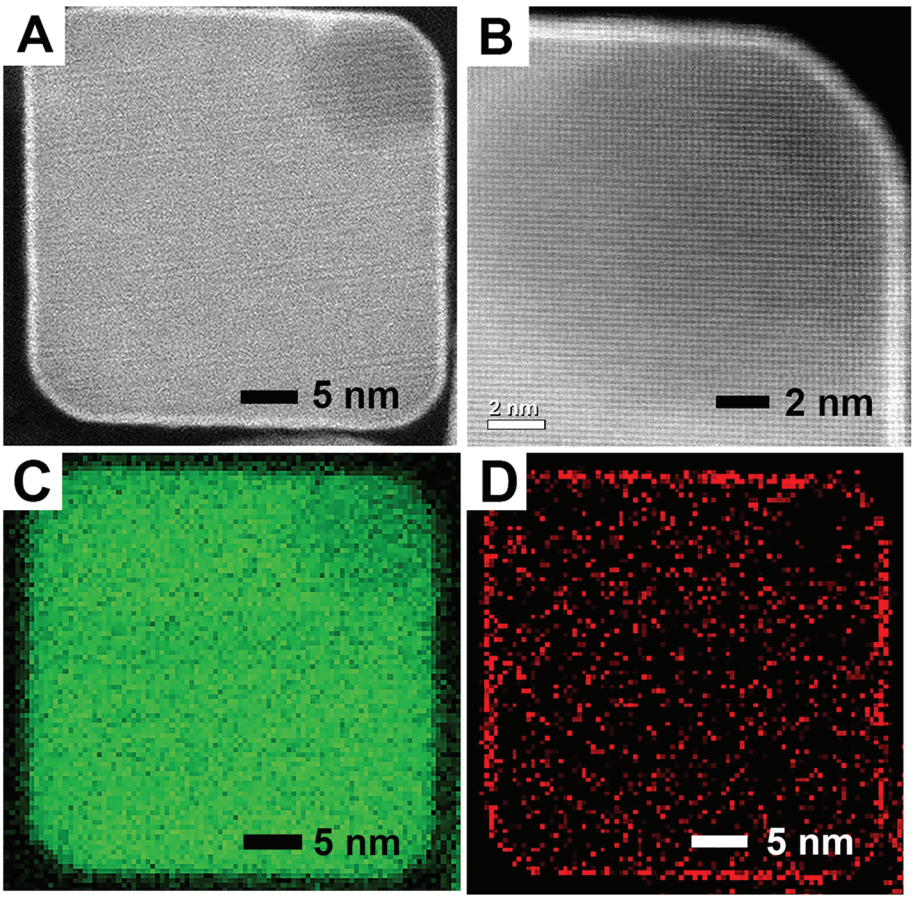

Fig. 3 (A, B) HAADF-STEM images, at two different magnifications, of a Ag@Pt nanocube shown in Fig. 2E. (C, D) STEM-EELS mapping of Ag (green) and Pt (red) for a Ag@Pt nanocube shown in (A).

We evaluated the catalytic activities of $Pt_{42}Ag_{58}$ nanocages toward ORR by benchmarking against a commercial Pt/C catalyst (46.6 wt%, 2.1 nm Pt particles supported on Ketjenblack EC-300J). Fig. 5A shows the cyclic voltammetry (CV) curves of the two catalysts in a N_2-saturated 0.1 M $HClO_4$ solution in the potential range of 0.08–1.10V_{RHE} at a scanning rate of 50 mV s^{-1}. The specific electrochemical active surface area (ECSA) of each catalyst was calculated from the charges associated with the desorption of hydrogen in the region of 0.08–0.45V_{RHE} by assuming the hydrogen monolayer desorption from Pt surfaces as 210 μC cm^{-2} for both catalysts. The ECSAs of the $Pt_{42}Ag_{58}$ nanocages and Pt/C are 32.16 m^2 g^{-1} and 52.30 m^2 g^{-1}, respectively. The lower specific ECSA of the $Pt_{42}Ag_{58}$ nanocages can be attributed to a number of factors, including the alloy composition, the intrinsically lower utilization efficiency of atoms for a 2D structure (*i.e.*, the side faces of the nanocages) compared to pseudo-spherical particles in Pt/C, and the aggregation of nanocages on the carbon. Fig. 5B shows the positive-going ORR polarization curves of both catalysts when we measured the ORR current densities of the catalysts in an O_2-saturated aqueous $HClO_4$ solution (0.1 M) in the potential range of 0.08–1.10V_{RHE} at a scanning rate of 10 mV s^{-1}. The kinetic currents of a polarization curve were then computed using the Koutecky–Levich equation and normalized to the ECSA and Pt mass of the catalyst to obtain the mass activity ($j_{k,mass}$) and specific activity ($j_{k,specific}$).[30] As shown in Fig. 5C and D, the $j_{k,mass}$ and $j_{k,specific}$ of the $Pt_{42}Ag_{58}$ nanocages were 0.30 A mg^{-1} and 0.93 mA cm^{-2}, respectively, at 0.9V_{RHE}, which are 1.6 and 2.5 times greater than those of the Pt/C catalyst at 0.18 A mg^{-1} and 0.37 mA cm^{-2}. After 5000 cycles of accelerated durability test, the composition of the Pt–Ag nanocages changed to $Pt_{89}Ag_{11}$ because of the selective dissolution of Ag during the potential cycling. As a result, both the mass activity and specific activity were decreased by 37% and 33%, respectively, while the specific ECSA was only reduced by 6.5%. Such composition-dependent activities of the Pt–Ag nanocages are consistent with those of Pt–Ag alloy nanocages prepared through a galvanic replacement reaction.[13] Our results also support the argument that the composition of Pt–Ag bimetallic nanocages plays an essential role in affecting the O–O bond breaking energetics, and ultimately the ORR activities. As shown in Fig. S8,† the morphology of the Pt–Ag nanocages remained the same before and after the durability test while their average edge length was reduced from 28.3 ± 2.7 nm to 23.8 ± 2.5 nm.

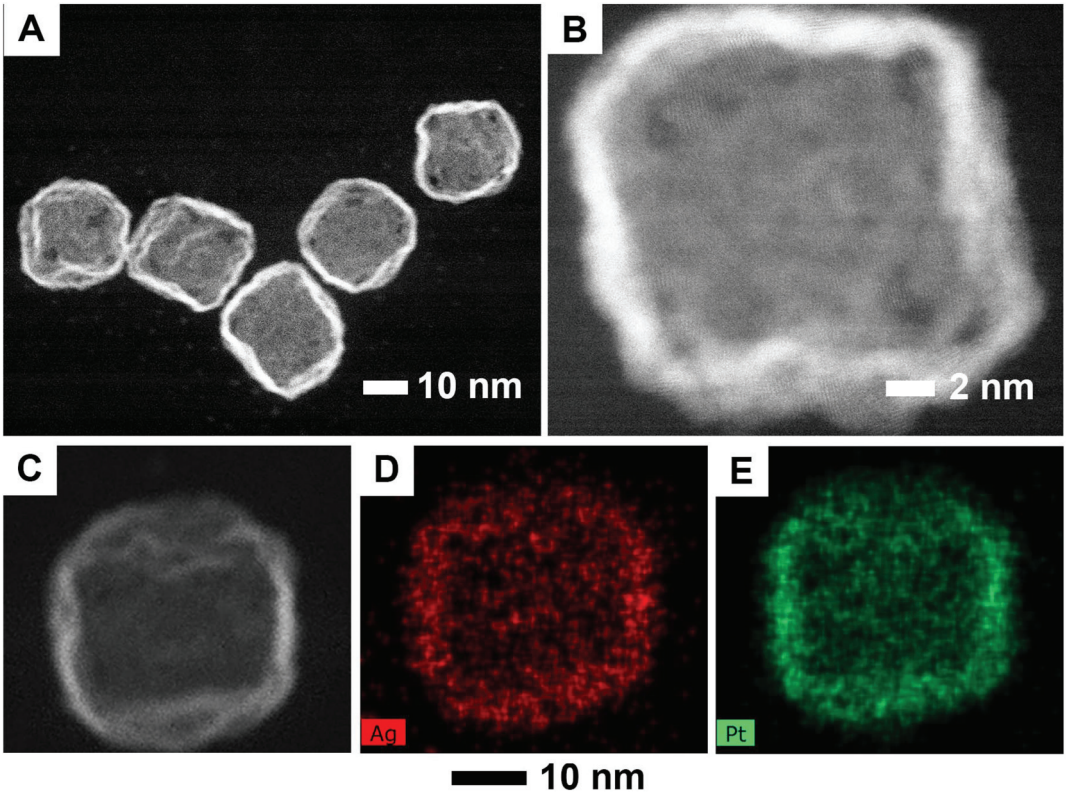

Fig. 4 (A) HAADF-STEM image of Pt–Ag nanocages shown in Fig. 2F. (B) Atomic resolution HAADF-STEM image of a nanocage and (C–E) STEM image and EDS mapping of Ag (red) and Pt (green) for an individual nanocage shown in (C).

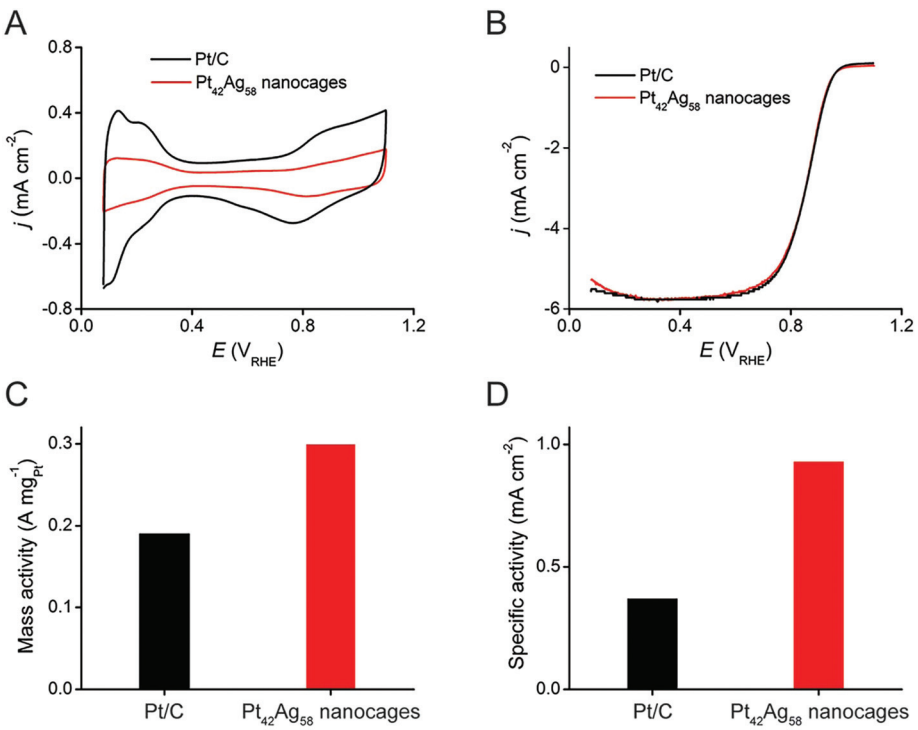

Fig. 5 (A) CV curves recorded from $Pt_{42}Ag_{58}$ nanocages and a commercial Pt/C catalyst. (B) Positive-going ORR polarization curves of $Pt_{42}Ag_{58}$ nanocages and a commercial Pt/C catalyst. The currents were normalized to the geometric area of the rotating disk electrode. (C) Mass activity and (D) specific activities of $Pt_{42}Ag_{58}$/C nanocages and a commercial Pt/C catalyst measured at $0.9V_{RHE}$.

Conclusions

In summary, we have demonstrated a facile and robust route to the fabrication of Pt–Ag nanocages with a wall thickness less than 2 nm using Ag nanocubes as the template. Our success relies on the establishment of a protocol for galvanic-free deposition of Pt on the surface of Ag nanocubes for the generation of Ag@Pt core–shell nanocubes with a shell thickness of three-atomic layers or roughly 0.6 nm. The synthetic protocol includes the one-shot injection of the H_2PtCl_6 precursor into an aqueous suspension of Ag nanocubes containing H_2Asc, NaOH, and PVP at an initial pH of 11.9. We demonstrated that the galvanic replacement reaction between the Ag nanocubes and H_2PtCl_6 was effectively suppressed because of the parallel reduction reaction involving $HAsc^-$. The Pt(IV) precursor would be reduced by $HAsc^-$ for the generation of Pt atoms, followed by their conformal deposition on the edges and then corners and side faces of Ag nanocubes in a layer-by-layer manner. After the removal of Ag cores using a wet etchant based on a mixture of $Fe(NO_3)_3$ and HNO_3, the core–shell nanocubes were transformed into Pt–Ag alloy nanocages with an ultrathin wall less than 2 nm. When the resultant nanocages with a composition of $Pt_{42}Ag_{58}$ were deposited on carbon and subjected to a catalytic test toward ORR, we obtained mass and specific activities of 0.30 A mg^{-1} and 0.93 mA cm^{-2}, which could be further improved by optimizing the elemental composition and surface structure of the Pt–Ag nanocages.

Conflicts of interest

There are no conflicts of interest.

Acknowledgements

This work was supported in part by the National Science Foundation (CHE-1412006), start-up funds from the Georgia Institute of Technology, and 3M non-tenured faculty award. Part of the research was performed at the Institute of Electronics and Nanotechnology. We acknowledge the use of electron microscopy resources at the Center for Functional Nanomaterials, a U.S. DOE Office of Science Facility, at Brookhaven National Laboratory under Contract No. DE-SC0012704. We thank Zhiheng Lyu at GT for her technical support to the electrochemical measurements.

Notes and references

1 J. M. Zalc, V. Sokolovskii and D. G. Löffler, *J. Catal.*, 2002, **206**, 169–171.
2 N. Tian, Z.-Y. Zhou, S.-G. Sun, Y. Ding and Z. L. Wang, *Science*, 2007, **316**, 732–735.
3 N. P. Brandon, S. Skinner and B. C. H. Steele, *Annu. Rev. Mater. Res.*, 2003, **33**, 183–213.
4 N. M. Marković and P. N. Ross Jr., *Surf. Sci. Rep.*, 2002, **45**, 117–229.
5 L. Zhang, L. T. Roling, X. Wang, M. Vara, M. Chi, J. Liu, S.-I. Choi, J. Park, J. A. Herron, Z. Xie, M. Mavrikakis and Y. Xia, *Science*, 2015, **349**, 412–416.
6 M. Jiang, B. Lim, J. Tao, P. H. C. Camargo, C. Ma, Y. Zhu and Y. Xia, *Nanoscale*, 2010, **2**, 2406–2411.
7 X. Wang, M. Vara, M. Luo, H. Huang, A. Ruditskiy, J. Park, S. Bao, J. Liu, J. Howe, M. Chi, Z. Xie and Y. Xia, *J. Am. Chem. Soc.*, 2015, **137**, 15036–15042.
8 X. Wang, L. Figueroa-Cosme, X. Yang, M. Luo, J. Liu, Z. Xie and Y. Xia, *Nano Lett.*, 2016, **16**, 1467–1471.
9 D. H. He, D. He, J. Wang, Y. Lin, P. Yin, X. Hong, Y. Wu and Y. Li, *J. Am. Chem. Soc.*, 2016, **138**, 1494–1497.
10 J. Chen, B. Wiley, J. McLellan, Y. Xiong, Z.-Y. Li and Y. Xia, *Nano Lett.*, 2005, **5**, 2058–2062.
11 Z. Peng, J. Wu and H. Yang, *Chem. Mater.*, 2010, **22**, 1098–1106.
12 W. Zhang, J. Yang and X. Lu, *ACS Nano*, 2012, **6**, 7397–7405.
13 X. Yang, L. T. Rolling, M. Vara, A. O. Elnabawy, M. Zhao, Z. D. Hood, S. Bao, M. Mavrikakis and Y. Xia, *Nano Lett.*, 2016, **16**, 6644–6649.
14 L. Wang and Y. Yamauchi, *J. Am. Chem. Soc.*, 2009, **131**, 9152–9153.
15 L. Wang and Y. Yamauchi, *J. Am. Chem. Soc.*, 2010, **132**, 13636–13638.
16 L. Wang, Y. Nemoto and Y. Yamauchi, *J. Am. Chem. Soc.*, 2011, **133**, 9674–9677.
17 L. Wang and Y. Yamauchi, *J. Am. Chem. Soc.*, 2013, **135**, 16762–16765.
18 Y. Wu, X. Sun, Y. Yang, J. Li and D. Qin, *Acc. Chem. Res.*, 2017, **50**, 1774–1784.
19 Y. Yin, J. Liu, Z.-W. Fu and D. Qin, *J. Am. Chem. Soc.*, 2014, **136**, 8153–8156.
20 J. Li, J. Liu, Y. Yang and D. Qin, *J. Am. Chem. Soc.*, 2015, **137**, 7039–7042.
21 X. Sun and D. Qin, *J. Mater. Chem. C*, 2015, **3**, 11833–11841.
22 Q. Zhang, W. Li, L. P. Wen, J. Chen and Y. Xia, *Chem. – Eur. J.*, 2010, **16**, 10234–10239.
23 A. T. Hubbard and F. C. Anson, *Anal. Chem.*, 1966, **38**, 58–61.
24 B. Shelimov, J. Lambert, M. Che and B. Didillon, *J. Am. Chem. Soc.*, 1999, **121**, 545–556.
25 P. J. Straney, L. E. Marbella, C. M. Andolina, N. T. Nuhfer and J. E. Millstone, *J. Am. Chem. Soc.*, 2014, **136**, 7873–7876.
26 T. Teranishi, M. Hosoe, T. Tanaka and M. Miyake, *J. Phys. Chem. B*, 1999, **103**, 3818–3827.
27 X. Sun, Y. Yang, Z. Zhang and D. Qin, *Chem. Mater.*, 2017, **29**, 4014–4021.
28 J. Li, X. Sun and D. Qin, *ChemNanoMat*, 2016, **2**, 494–499.
29 Y. Zhang, J. Liu, J. Ahn, T.-H. Xiao, Z.-Y. Li and D. Qin, *ACS Nano*, 2017, **11**, 5080–5086.
30 B. Lim, M. Jiang, P. H. C. Camargo, E. C. Cho, J. Tao, X. Lu, Y. Zhu and Y. Xia, *Science*, 2009, **324**, 1302–1305.

